

Impact of hyperons on structural properties of neutron stars and hybrid stars within four-dimensional Einstein-Gauss-Bonnet gravity

Ishfaq Ahmad Rather¹, Grigoris Panotopoulos²

^a[§]¹*Institute for Theoretical Physics Goethe University 60438 Frankfurt am Main Germany*

^b[§]²*Departamento de Ciencias Fisicas Universidad de la Frontera Casilla 54-D 4811186 Temuco Chile*

Abstract

We investigate the impact of hyperons and phase transition to quark matter on the structural properties of neutron stars within the four-dimensional Einstein-Gauss-Bonnet gravity (EGB). We employ the density-dependent relativistic mean-field model (DDME2) for the hadronic phase and the density-dependent quark mass (DDQM) model for the quark phase to construct hadronic and hybrid equations of state (EoSs) that are consistent with the astrophysical constraints. The presence of hyperons softens the EoS and with a phase transition, the EoS further softens and the speed of sound squared drops to around 0.2 for the maximum mass configuration which lies in the pure quark phase. Adjusting the Gaussian-Bonnet coupling constant α within its allowed range results in a decrease in the mass-radius relationship for negative α , and an increase for positive α . In addition, functions are fitted to the maximum mass and its associated radius as a function of constant α to observe its impact on these properties.

Keywords: Neutron Star, Equation-of-State, Hyperons, Quark Matter, Phase Transition, Theories of gravity other than GR.

1. Introduction

The question “How many dimensions are there?” is one of the fundamental questions modern theoretical physics tries to answer. This is due to the fact that although our observable Universe is clearly four-dimensional (4D), advances in High Energy Physics from the 20’s as well as over the last decades, such as Kaluza-Klein theories [1, 2], Supergravity [3] and Superstring/M-Theory [4, 5] suggest that extra spatial dimensions might exist. In addition to that, in more than four dimensions higher order curvature terms are natural in Lovelock theory [6], while higher order curvature corrections appear in the low-energy effective actions of Superstring Theory [7].

As is well-known, in four-dimensional space-times the Gauss-Bonnet (GB) term is a topological invariant, and as such it does not contribute to the equations of motion. However, a few years ago a novel 4D Einstein-Gauss-Bonnet (EGB) theory of gravity was proposed by Glavan and Lin [8]. They showed that even in four dimensions there are non-trivial effects coming from the presence of the GB term. The authors’ basic idea was to rescale the GB coupling constant by $\alpha \rightarrow \alpha/(D-4)$ in D dimensions, and then take the limit $D \rightarrow 4$. As a consequence of the procedure, it turned out that one can bypass the conclusions of Lovelock’s theorem, and thus avoid the Ostrogradsky instability [9]. The resultant theory is now dubbed as the novel 4D EGB theory, and it has attracted a lot of attention as well as some criticism. Since then, a number of black hole solutions have been found within that theory, and their physical

properties have been investigated. For an incomplete list see e.g. [10, 11, 12, 13, 14, 15, 16], charged black holes [17, 18], black holes coupled to magnetic charges and non-linear Electrodynamics [19, 20, 21]. Besides that, deflection of light by black holes [22, 23, 24], quasi-normal modes [25, 26, 27] and shadow casts by black holes [28, 29, 30] have been investigated as well. Moreover, Morris-Thorne-like wormholes and thin-shell wormholes have been investigated in [31, 32]. In Ref. [33] it was shown that in order to have a well-defined linearized theory, the geometry must be (locally) conformally flat. In view of the importance of that theory, research has been conducted in order to constrain the new re-scaled Gauss-Bonnet parameter using observational data, see for instance [34, 35, 36] and references therein.

Neutron stars, with radii around 10 km and masses of 2 solar masses or more, are composed of extremely dense hadronic matter, making them ideal for examining cold, dense nuclear matter. Theoretical predictions of their composition and properties like mass and radius depend on the nuclear equation of state (EoS). Neutron stars contain protons to maintain chemical equilibrium, but due to the strong interaction’s nonperturbative nature, the exact EoS is not well understood. This makes the precise structure of neutron stars at high densities, where exotic forms of matter may exist, unknown. Comparing theoretical models to astrophysical data helps to clarify the real EoS of cold dense nuclear matter. Theoretical models of neutron stars usually include not just nucleons but also hyperons to account for energy considerations [37]. However, adding hyperons tends to soften the EoS, reducing the neutron star’s maximum possible mass and contributing to the “hyperon puzzle”[38].

At extremely high densities, a transition from hadronic mat-

Email addresses: rather@astro.uni-frankfurt.de (Ishfaq Ahmad Rather¹), grigorios.panotopoulos@ufroterra.cl (Grigoris Panotopoulos²)

ter to quark matter could happen, leading to a hybrid star with a quark core and hadronic shell. This hadron-quark transition is a significant prediction of QCD under extreme conditions. Gravitational waves from neutron star mergers provide important information to help understand the EoS and provide insights into neutron star interiors, including possible quark matter. The oscillations of neutron stars, observable in gravitational wave frequencies, reveal details about the internal structure and possible presence of quark matter, aiding our understanding of dense cosmic matter [39, 40].

The stellar properties for the NS obtained from the EoSs for several different models for the hadronic matter as well as quark matter need to satisfy several astrophysical constraints for the mass and radii. The most important constant on the EoS comes from the mass measurements of massive pulsars such as J1614-2230 ($M = 1.97 \pm 0.04 M_\odot$) [41], PSR J0348+0432 ($M = 2.01 \pm 0.04 M_\odot$) [42], and PSR J0740+6620 ($M = 2.08 \pm 0.07 M_\odot$) [43] which suggest that the EoS of dense matter must be able to describe neutron stars of $2 M_\odot$ implying that the matter should remain sufficiently stiff at high densities. Additionally, X-ray measurements of the radius of pulsars from the Neutron Star Interior Composition Explorer (NICER) and X-ray Multi-Mirror (XMM) constrain the radius to $R = 12.39^{+1.30}_{-0.98}$ km [44] and $R = 13.7^{+2.6}_{-1.5}$ km [45]. Recent analysis provided an updated values of these measurements to $R = 12.49^{+1.28}_{-0.88}$ [46], and $R = 12.76^{+1.49}_{-1.02}$ [47]. The radius measurements for the PSR J0030+0451 at $1.4 M_\odot$ are, $R = 13.02^{+1.24}_{-1.06}$ km by Miller *et al.* [48] and $R = 12.71^{+1.14}_{-1.19}$ km by Riley *et al.* [49]. These two limits include the recent measurement by Vinciguerra *et al.* [50]. The mass-radius measurement of PSR J0437-4715 to $R = 11.36^{+0.95}_{-0.63}$ km for a mass of $M = 1.418 \pm 0.037 M_\odot$ by Choudhury *et al.* [51] favors softer EoS models. Moreover, low mass and radius measurements of the object such as HESS J1731-347 with very low mass $M = 0.77^{+0.20}_{-0.17} M_\odot$ and radius $R = 10.4^{+0.86}_{-0.78}$ km [52], and XTE J1814-338 with a mass and radius of $M = 1.21^{+0.05}_{-0.05} M_\odot$ and $R = 7.^{+0.4}_{-0.4}$ km [53] challenge existing EoS models. The EoS not fulfilling such constraints, especially the $2 M_\odot$ are ruled out.

In the present work, we propose to investigate some astrophysical implications of the four-dimensional Einstein-Gauss-Bonnet gravity. To be more precise, we shall study the impact of the Gauss-Bonnet coupling constant α on the mass-radius relationships of hadronic and hybrid stars, including hyperons. The plan of our work is as follows: In Section 2, we present the theory and the structure equations for non-rotating stars. In Section 3, we discuss the equation of state (EoS) of hadronic matter, deconfined quark matter, and phase transition. Section 4 presents and discusses our main numerical results for different EoS with different GB constant values. Finally, we summarize our work in section 5. Throughout the manuscript, we adopt the mostly positive metric signature, and we work in geometrical units where Newton's constant and the speed of light in a vacuum are set to unity, $G = 1 = c$.

2. Relativistic Stars within 4D EGB Gravity

In this section, we give a brief review of the 4D EGB gravity, and present the field equations as well as the structure equations for stellar interior solutions following closely [54].

The starting point is the action in D -dimensions, which can be written down as follows

$$S = \frac{c^4}{16\pi} \int_{\mathcal{M}} d^D x \sqrt{-g} \left(R + \frac{\alpha}{D-4} \mathcal{L}_{\text{GB}} \right) + \mathcal{S}_M[g], \quad (1)$$

where R is the Ricci scalar, g is the determinant of the metric tensor $g_{\mu\nu}$, while $R_{\mu\nu}$ and $R_{\mu\sigma\nu\rho}$ are the Ricci tensor and the Riemann tensor, respectively. The GB coupling constant α has dimension of $[length]^2$, and \mathcal{L}_{GB} is the GB term, defined by

$$\mathcal{L}_{\text{GB}} \equiv R^{\mu\nu\rho\sigma} R_{\mu\nu\rho\sigma} - 4R^{\mu\nu} R_{\mu\nu} + R^2. \quad (2)$$

In Eq. (1), the \mathcal{S}_M is the action of matter content, which does not depend on the derivatives of the metric tensor. The variation of (1) with respect to the metric tensor, $g_{\mu\nu}$, leads to the following field equations

$$G_{\mu\nu} + \frac{\alpha}{D-4} H_{\mu\nu} = 8\pi T_{\mu\nu}, \quad (3)$$

where the Einstein tensor $G_{\mu\nu}$ and Lanczos tensor $H_{\mu\nu}$ are defined by

$$\begin{aligned} G_{\mu\nu} &\equiv R_{\mu\nu} - \frac{1}{2} R g_{\mu\nu}, \\ H_{\mu\nu} &\equiv 2 \left(R R_{\mu\nu} - 2 R_{\mu\sigma} R^{\sigma}_{\nu} \right. \\ &\quad \left. - 2 R_{\mu\sigma\nu\rho} R^{\sigma\rho} - R_{\mu\sigma\rho\delta} R^{\sigma\rho\delta}_{\nu} \right) - \frac{1}{2} g_{\mu\nu} \mathcal{L}_{\text{GB}}, \end{aligned} \quad (4)$$

while the energy-momentum tensor of matter distribution is defined by

$$T_{\mu\nu} = - \frac{2}{\sqrt{-g}} \frac{\delta \left(\sqrt{-g} \mathcal{L}_m \right)}{\delta g^{\mu\nu}}, \quad (5)$$

Note that in action (1) we have rescaled the coupling constant $\alpha \rightarrow \alpha/(D-4)$. As a result the above theory does not suffer from the Ostrogradski instability, and that way a novel 4D EGB gravity can be redefined in the limit $D \rightarrow 4$ [8].

Next, taking the limit $D \rightarrow 4$ and considering static, spherically symmetric interior solutions describing hydrostatic equilibrium of stars we choose the metric of the following form in Schwarzschild-like coordinates t, r, θ, φ

$$ds^2 = -e^{2\Phi(r)} dt^2 + e^{2\Lambda(r)} dr^2 + r^2 d\Omega_2^2, \quad (6)$$

where $d\Omega_2^2 = d\theta^2 + \sin^2\theta d\varphi^2$ is the metric of the unit 2-dimensional sphere, while the metric functions $\Phi(r)$ and $\Lambda(r)$ depend only on the radial coordinate r . Here we are interested in non-rotating stars made of isotropic matter, the energy-momentum tensor of which in $(3+1)$ -dimensional space-times may be written down as follows

$$T_{\mu\nu} = (\epsilon + P) u_\mu u_\nu + P g_{\mu\nu}, \quad (7)$$

where u^μ is the four-velocity, $\rho = \rho(r)$ is the energy density, and $P = P(r)$ is the pressure of the fluid. Thus, in the limit $D \rightarrow 4$ the non-zero components of the field equations are the following

$$\begin{aligned} \frac{2}{r} \frac{d\Lambda}{dr} &= e^{2\Lambda} \left[\frac{8\pi G}{c^4} \epsilon(r) - \frac{1 - e^{-2\Lambda}}{r^2} \left(1 - \frac{\alpha(1 - e^{-2\Lambda})}{r^2} \right) \right] \\ &\quad \times \left[1 + \frac{2\alpha(1 - e^{-2\Lambda})}{r^2} \right]^{-1}, \\ \frac{2}{r} \frac{d\Phi}{dr} &= e^{2\Lambda} \left[\frac{8\pi G}{c^4} P(r) + \frac{1 - e^{-2\Lambda}}{r^2} \left(1 - \frac{\alpha(1 - e^{-2\Lambda})}{r^2} \right) \right] \\ &\quad \times \left[1 + \frac{2\alpha(1 - e^{-2\Lambda})}{r^2} \right]^{-1}, \\ \frac{dP}{dr} &= -(\epsilon + P) \frac{d\Phi}{dr}. \end{aligned} \quad (9)$$

To recast the generalized TOV equations into a more familiar form, we replace the metric function by the following expression $e^{-2\Lambda} = 1 - \frac{2Gm(r)}{c^2 r}$, which represents the gravitational mass within the sphere of radius r . After some algebraic manipulation, the fluid equation takes the following form

$$\frac{dP(r)}{dr} = -\frac{G\epsilon(r)m(r)}{c^2 r^2} \frac{\left[1 + \frac{P(r)}{\epsilon(r)} \right] \left[1 + \frac{4\pi r^3 P(r)}{c^2 m(r)} - \frac{2G\alpha m(r)}{c^2 r^3} \right]}{\left[1 + \frac{4G\alpha m(r)}{c^2 r^3} \right] \left[1 - \frac{2Gm(r)}{c^2 r} \right]}. \quad (10)$$

imposing the condition $P(0) = P_c$ at the center of the fluid sphere, with P_c being the central pressure. It is not difficult to see that one may recover the standard TOV equations of Einstein's General Relativity for isotropic fluid distributions when $\alpha \rightarrow 0$.

The first structure equation can be rewritten in terms of the mass function $m(r)$ as follows

$$m'(r) = \frac{6\alpha Gm(r)^2 + 4\pi r^6 \epsilon(r)}{4\alpha Gm(r) + c^2 r^4}, \quad (11)$$

where a prime denotes differentiation with respect to radial coordinate. Here, we impose $m(r = 0) = 0$ to be the appropriate condition at the center of the fluid sphere. Furthermore, as it is more convenient to work with dimensionless variables, we introduce the following set of dimensionless functions: $P(r) = \epsilon_0 \tilde{P}(r)$ and $\epsilon(r) = \epsilon_0 \tilde{\epsilon}(r)$ and $m(r) = M_\odot \tilde{M}(r)$, with $\epsilon_0 = 1 \text{ MeV/fm}^3$. After a short calculation, the above two equations take now the form

$$\frac{d\tilde{P}(r)}{dr} = -\frac{c_1 \tilde{\epsilon}(r) \tilde{M}(r)}{r^2} \frac{\left[1 + \frac{\tilde{P}(r)}{\tilde{\epsilon}(r)} \right] \left[1 + \frac{c_2 r^3 \tilde{P}(r)}{\tilde{M}(r)} - \frac{2c_1 \alpha \tilde{M}(r)}{r^3} \right]}{\left[1 + \frac{4c_1 \alpha \tilde{M}(r)}{r^3} \right] \left[1 - \frac{2c_1 \tilde{M}(r)}{r} \right]}, \quad (12)$$

and

$$\frac{d\tilde{M}(r)}{dr} = \frac{6c_1 \alpha \tilde{M}(r)^2 + c_2 r^6 \tilde{\epsilon}(r)}{4c_1 \alpha r \tilde{M}(r) + r^4}, \quad (13)$$

where we have defined the constants $c_1 \equiv \frac{GM_\odot}{c^2} = 1.474 \text{ km}$ and $c_2 \equiv \frac{4\pi\epsilon_0}{M_\odot c^2} = 1.125 \times 10^{-5} \text{ km}^{-3}$. The structure equations can be integrated numerically imposing the appropriate initial

conditions at the center of the star, $r \rightarrow 0$, for a given EoS $P = P(\epsilon)$ that relates the pressure to the energy density.

From now on we adopt geometrical units, i.e. $G = 1 = c$. To obtain interior solutions describing hydrostatic equilibrium, we need to derive an equation of state, and this is the subject of the next section. We vary the GB parameter in the range $[-5 \text{ km}^2, +5 \text{ km}^2]$ following [55], and we impose the following matching conditions

$$P(R) = 0, \quad 1 - 2\frac{m(R)}{R} = f(R) \quad (14)$$

at the surface of the star, $r \rightarrow R$, with R being the stellar radius. The function $f(r)$ is the metric function of the exterior vacuum solution [56]

$$f(r) = 1 + \frac{r^2}{2\alpha} \left[1 - \sqrt{1 + \frac{8\alpha M}{r^3}} \right], \quad (15)$$

which generalizes the Schwarzschild geometry of GR in the absence of matter, and where M is the stellar mass. Clearly in the limit $\alpha \rightarrow 0$ we recover the Schwarzschild solution.

3. Equation-of-State Formalism

3.1. Hadronic matter

To analyze how the Gauss-Bonnet (GB) constant α impacts the mass-radius relationship of neutron stars (NS), we utilize a density-dependent relativistic mean-field (DD-RMF) model to describe hadronic matter. This model is acclaimed for accurately replicating the experimental features of nuclear matter and aligning with astrophysical constraints. It involves interactions between nucleons and other hadrons through virtual meson exchanges. The particular DD-RMF model applied includes interactions with the scalar meson σ , vector mesons ω and ϕ , and the isovector-vector meson ρ .

In any RMF theory, the Lagrangian density serves as the fundamental assumption, incorporating components from free baryons, mesons, and their interaction terms. Through the mean-field approximation, the Lagrangian used for the relativistic model in describing hadronic interactions is represented by

$$\begin{aligned} \mathcal{L}_{\text{DD-RMF}} &= \sum_{b \in H} \bar{\psi}_b \left[i\gamma^\mu \partial_\mu - \gamma^0 (g_{\omega b} \omega_0 + g_{\phi b} \phi_0 + g_{\rho b} I_{3b} \rho_{03}) \right. \\ &\quad \left. - (m_b - g_{\sigma b} \sigma_0) \right] \psi_b + \sum_l \bar{\psi}_l (i\gamma^\mu \partial_\mu - m_l) \psi_l \\ &\quad - \frac{1}{2} m_\sigma^2 \sigma_0^2 + \frac{1}{2} m_\omega^2 \omega_0^2 + \frac{1}{2} m_\phi^2 \phi_0^2 + \frac{1}{2} m_\rho^2 \rho_{03}^2. \end{aligned} \quad (16)$$

The first sum in the above equation represents the Dirac-type interacting Lagrangian for the spin-1/2 baryon octet, $H = \{n, p, \Lambda, \Sigma^-, \Sigma^0, \Sigma^+, \Xi^-, \Xi^0\}$. The second term describes the contribution from leptons in the hadronic matter as a free non-interacting fermion gas, $l = \{e, \mu\}$, as their contribution is necessary to ensure the β -equilibrium and charge neutrality essential to stellar matter. The remaining terms account for the purely mesonic part of the Lagrangian.

In DD-RMF models, coupling constants depend on scalar or vector densities, with vector density commonly parameterized to impact self-energy alone [57]. We utilize the DD-RMF parametrization DDME2, where meson couplings scale with the baryonic density factor $\eta = n_B/n_0$ obeying the function

$$g_{ib}(n_B) = g_{ib}(n_0) \frac{a_i + b_i(\eta + d_i)^2}{a_i + c_i(\eta + d_i)^2} \quad (17)$$

for $i = \sigma, \omega, \phi$ and

$$g_{\rho b}(n_B) = g_{\rho b}(n_0) \exp[-a_\rho(\eta - 1)], \quad (18)$$

for $i = \rho$.

Table 1: The parameters of the DDME2 set (top) and its predictions to the nuclear matter properties at saturation density (bottom).

i	$m_i(\text{MeV})$	a_i	b_i	c_i	d_i	$g_{iN}(n_0)$
σ	550.1238	1.3881	1.0943	1.7057	0.4421	10.5396
ω	783	1.3892	0.9240	1.4620	0.4775	13.0189
ρ	763	0.5647	—	—	—	7.3672

Quantity	Constraints [58, 59]	DDME2
n_0 (fm^{-3})	0.148–0.170	0.152
$-B/A$ (MeV)	15.8–16.5	16.4
K_0 (MeV)	220–260	252
S_0 (MeV)	31.2–35.0	32.3
L_0 (MeV)	38–67	51

The model's parameters are determined using experimental constraints on nuclear matter near its saturation density n_0 , focusing on the binding energy B/A , compressibility modulus K_0 , symmetry energy S_0 , and its slope L_0 , as presented in Table 1. These parameters are tailored for pure nucleonic matter, comprised solely of protons and neutrons. To establish the meson couplings for other hadronic species, we define the ratio $\chi_{ib} = g_{ib}/g_{iN}$ for the baryon coupling relative to the nucleon coupling, with $i = \{\sigma, \omega, \phi, \rho\}$. In this study, hyperons are included in the nucleonic matter, and we follow the methodology of Lopes et al. [60] to calculate their respective χ_{ib} ratios. This formalism maintains a consistent framework based on symmetry principles, particularly ensuring that the Yukawa coupling terms in the Lagrangian density of DD-RMF models are invariant under SU(3) and SU(6) group transformations. Consequently, the couplings are adjusted to achieve the potentials $U_\Lambda = -28$ MeV, $U_\Sigma = 30$ MeV, and $U_\Xi = -4$ MeV using a single free parameter α_V . We choose $\alpha_V = 1.0$ for the baryon-meson coupling scheme, which corresponds to an unbroken SU(6) symmetry, and the values of χ_{ib} are given in Table 2, considering the isospin projections in the Lagrangian terms [61].

From Eq. (16), thermodynamic quantities can be calculated in the standard way for RMF models. The baryonic density of a baryon of the species b is given by

$$n_b = \frac{\lambda_b}{2\pi^2} \int_0^{k_{Fb}} dk k^2 = \frac{\lambda_b}{6\pi^2} k_{Fb}^3, \quad (19)$$

Table 2: Baryon-meson coupling constants χ_{ib} [60].

b	$\chi_{\omega b}$	$\chi_{\sigma b}$	$I_{3b}\chi_{\rho b}$	$\chi_{\phi b}$
Λ	2/3	0.611	0	0.471
$\Sigma^-, \Sigma^0, \Sigma^+$	2/3	0.467	-1, 0, 1	-0.471
Ξ^-, Ξ^0	1/3	0.284	-1/2, 1/2	-0.314

where k_F denotes the Fermi momentum since we assume the stellar matter to be at zero temperature and λ_b is the spin degeneracy factor. The effective masses are given by

$$m_b^* = m_b - g_{\sigma b}\sigma_0. \quad (20)$$

Solving the energy-momentum tensor, we obtain the energy density as

$$\begin{aligned} \varepsilon_B = & \sum_b \frac{\gamma_b}{2\pi^2} \int_0^{k_{Fb}} dk k^2 \sqrt{k^2 + m_b^{*2}} \\ & + \sum_l \frac{1}{\pi^2} \int_0^{k_{Fl}} dk k^2 \sqrt{k^2 + m_l^2} + \frac{m_\sigma^2}{2} \sigma_0^2 + \frac{m_\omega^2}{2} \omega_0^2 \\ & + \frac{m_\phi^2}{2} \phi_0^2 + \frac{m_\rho^2}{2} \rho_{03}^2. \end{aligned} \quad (21)$$

The effective chemical potentials become

$$\mu_b^* = \mu_b - g_{\omega b}\omega_0 - g_{\rho b}I_{3b}\rho_{03} - g_{\phi b}\phi_0 - \Sigma^r, \quad (22)$$

where Σ^r is the rearrangement term arising due to the density-dependent couplings and is necessary to ensure thermodynamical consistency. The form is

$$\Sigma^r = \sum_b \left[\frac{\partial g_{\omega b}}{\partial n_b} \omega_0 n_b + \frac{\partial g_{\rho b}}{\partial n_b} \rho_{03} I_{3b} n_b + \frac{\partial g_{\phi b}}{\partial n_b} \phi_0 n_b - \frac{\partial g_{\sigma b}}{\partial n_b} \sigma_0 n_b^s \right], \quad (23)$$

The μ_b are determined by the chemical equilibrium condition

$$\mu_b = \mu_n - q_b \mu_e, \quad (24)$$

in terms of the chemical potential of the neutron and the electron, with $\mu_\mu = \mu_e$. The particle populations of each individual species are determined by Eq. (24) together with the charge neutrality condition of $\sum_i n_i q_i = 0$, where q_i is the charge of the baryon or lepton i .

The expression for pressure can be written in terms of the energy density and the chemical potential as

$$P = \sum_i \mu_i n_i - \epsilon + n_B \Sigma^r, \quad (25)$$

which receives a correction from the rearrangement term to guarantee thermodynamic consistency and energy-momentum conservation [62, 63].

3.1.1. Deconfined quark matter

We utilize the density-dependent quark mass (DDQM) model to represent quark matter. This straightforward and adaptable framework is ideal for exploring the deconfinement phase transition in hybrid stars, as referenced in [64]. The DDQM model emulates QCD quark confinement using quark masses that depend on density, defined by

$$m_q = m_{q0} + \frac{D}{n_B^{1/3}} + C n_B^{1/3} = m_{q0} + m_Q, \quad (26)$$

where m_{q0} ($q = u, d, s$) corresponds to the current mass of the q th quark, n_B is the baryon number density, and m_Q corresponds to the density-dependent term that encompasses the interaction between quarks. The model parameters D and C dictate linear confinement and the leading-order perturbative interactions, respectively [65].

Careful treatment is needed to maintain thermodynamic consistency when introducing density dependence for state variables such as density, temperature, or magnetic field, similar to the method in Eq. (23) for the DD-RMF model. We use the formalism from [65] to ensure thermodynamic consistency in DDQM. At zero temperature, the basic energy density differential relationship is described as follows:

$$d\varepsilon = \sum_q \mu_q dn_q, \quad (27)$$

where ε represents the matter contribution to the energy density of the system, μ_q are the particle chemical potentials and n_q are the particle densities, respectively.

Expressing this model in terms of effective chemical potentials, we write the energy density for a free system as

$$\varepsilon = \Omega_0(\{\mu_q^*, \{m_q\}\}) + \sum_q \mu_q^* n_q, \quad (28)$$

using the density-dependent quark masses $m_q(n_B)$ and effective chemical potentials μ_q^* . The Ω_0 is the thermodynamic potential of a free system. Differentiating this form to yield

$$d\varepsilon = d\Omega_0 + \sum_q \mu_q^* dn_q + \sum_q n_q d\mu_q^*. \quad (29)$$

We can then write $d\Omega_0$ as

$$d\Omega_0 = \sum_q \frac{\partial \Omega_0}{\partial \mu_q^*} d\mu_q^* + \sum_q \frac{\partial \Omega_0}{\partial m_q} dm_q, \quad (30)$$

with

$$dm_q = \sum_j \frac{\partial m_q}{\partial n_j} dn_j, \quad (31)$$

where, in order to ensure thermodynamic consistency, the densities are connected to the effective chemical potentials by the relation

$$n_q = - \frac{\partial \Omega_0}{\partial \mu_q^*}. \quad (32)$$

Eq. (29) can thus be rewritten as

$$d\varepsilon = \sum_q \left(\mu_q^* + \sum_j \frac{\partial \Omega_0}{\partial m_j} \frac{\partial m_j}{\partial n_q} \right) dn_q, \quad (33)$$

providing a relation between the real and effective chemical potentials,

$$\mu_q = \mu_q^* + \sum_j \frac{\partial \Omega_0}{\partial m_j} \frac{\partial m_j}{\partial n_q}. \quad (34)$$

The pressure P for the system can be obtained from the fundamental relation $P = -\varepsilon + \sum_q \mu_q n_q$, as:

$$P = -\Omega_0 + \sum_{q,j} \frac{\partial \Omega_0}{\partial m_j} n_q \frac{\partial m_j}{\partial n_q}, \quad (35)$$

yielding a thermodynamically consistent EoS for quark matter.

3.1.2. Phase transition

The characteristics of the transition are influenced by the quark and hadron EoS models utilized. This study assumes the hadron-quark deconfinement transition to be a first-order phase transition, as effective models in the QCD phase diagram's high-density sector suggest. A phase transition can manifest as either a Maxwell [66] or mixed (Gibbs) [67] phase transition, determined by the hadron-quark phase surface tension. In Maxwell construction, the phases remain distinct, ensuring local charge conservation, whereas, in Gibbs construction, quarks and hadrons coexist over a range of baryonic densities with global charge conservation. The thermodynamic process involves aligning the EoS of both phases and pinpointing the coexistence point. The method chosen for mixed-phase construction affects the stellar properties of the associated EoS [68, 69].

For this work, we utilize the Maxwell construction to develop a hybrid EoS featuring a first-order phase transition at specific critical values of baryonic chemical potential and pressure. As per Gibbs' criteria, the transition takes place at the point where

$$P^{(i)} = P^{(f)} = P_0, \quad (36)$$

$$\mu^{(i)}(P_0) = \mu^{(f)}(P_0) = \mu_0, \quad (37)$$

sets the transition between the initial (i) and final (f) homogeneous phases with

$$\mu^{(i,f)} = \frac{\varepsilon^{(i,f)} + P^{(i,f)}}{n_B^{(i,f)}}, \quad (38)$$

where $\varepsilon^{(i,f)}$, $P^{(i,f)}$ and $n_B^{(i,f)}$ are the total energy density, pressure, and baryon number density, obtained from the EoS of each phase. The conditions above the values of P_0 and μ_0 are to be determined from the equations of state of both hadronic and deconfined quark phases. The transition point location, for a given baryonic composition in the hadronic phase, will be notably influenced by the choice of the free parameters for the DDQM model [64]. In this study, we used a particular set of $(C, D^{1/2})$ for pure nucleonic EoS and another set for hypersonic EoS. The choice of these parameters is explained in [70].

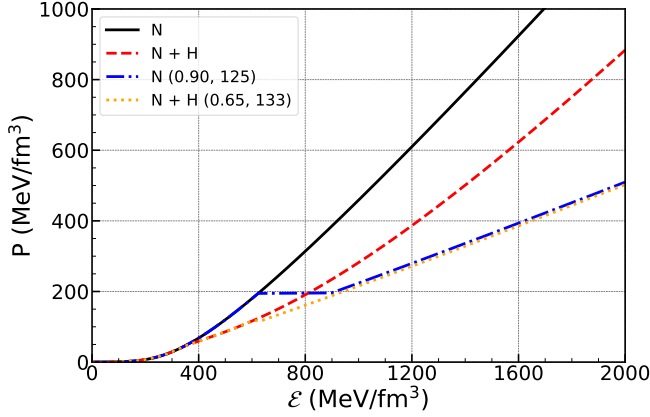


Figure 1: Energy density and pressure variation for the given DD-ME2 parameter set without and with a phase transition to the quark matter at different quark model parameters ($C, D^{1/2}$). The solid (dashed) line represents the pure nucleonic matter (nucleonic matter with hyperons) without a phase transition, while as dash-dotted (dotted) line represents the EoS for the nucleonic matter (nucleonic with hyperons) with a phase transition.

4. Numerical results and discussion

Figure 1 illustrates how pressure varies with energy density (EoS) for a neutron star under beta-equilibrium and charge-neutral conditions. The solid line corresponds to the EoS with nucleons only (N) while as the dashed line corresponds to the EoS with nucleons and hyperons (N + H). The dash-dotted and dotted lines correspond to the hybrid EoS with nucleons only, N (0.90, 125), and nucleons with hyperons, N + H (0.65, 133), where the numbers in the brackets correspond to the specific choice of quark model parameters ($C, D^{1/2}$). The EoS for the pure nucleonic EoS is very stiff implying that the rise in the pressure for a given energy density is very large. For the EoS with hyperons, N + H, we see that the low density part remains unchanged. The point where the EoS starts to deviate from the pure nucleonic one, around 380 MeV/fm³, marks the appearance of hyperons that softens the EoS.

Regarding the hybrid EoSs, we see that the hybrid nucleonic EoS, N (0.90, 125), has a sharp transition where the pressure is constant, shifts to the quark matter EoS with a mixed phase region from around 600 MeV/fm³ to 900 MeV/fm³, a jump of 300 MeV/fm³. The presence of hyperons causes a shift in the coexistence point towards lower density, marking a mixed-phase region of around 80 MeV/fm³. Thus, for hybrid N EoS, the phase transition takes place at a very high density compared to hybrid N + H EoS. For the hybrid N + H EoS, the hadron-quark phase transition region is small and occurs at low density compared to the others. This implies a large quark phase present in comparison to the other hybrid EoSs. Post-phase transition, the EoS at higher densities is much more uniform compared to its hadronic counterpart. For instance, the parameter set ($C, D^{1/2}$) = (0.90, 125 MeV) results in only a slightly stiffer EoS than ($C, D^{1/2}$) = (0.65, 133 MeV). However, the position of the coexistence point plays the most crucial role when constructing the hybrid EoS.

For a full unified EoS with crust part, we use the Baym-

Pethick-Sutherland (BPS) EoS [71] for the outer crust, while the inner crust EoS is generated using the DD-ME2 parameter set in the Thomas-Fermi approximation [72, 73, 74].

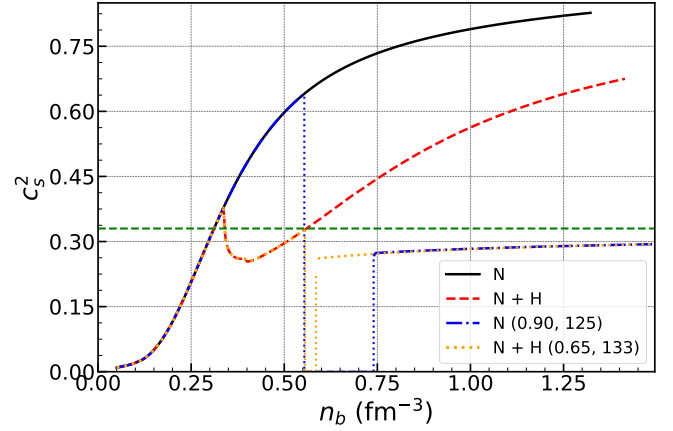


Figure 2: Speed of sound squared as a function of number density for the different hadronic composition EoS without (N, N + H) and with phase transition (N (0.90, 125), N + H (0.65, 133)) to the quark matter. The dotted lines in the right plot correspond to the mixed-phase region where c_s^2 drops to zero. The green dashed line in both plots represents the conformal limit $c_s^2 = 1/3$.

Figure 2 shows the speed of sound squared as a function of number density for different compositions of the matter studied in this work, without and with a phase transition. From the thermodynamic stability, we need to ensure that $c_s^2 > 0$ and from the causality, we have an absolute bound, $c_s^2 \leq 1$. For very high densities, perturbative QCD findings anticipate an upper limit of $c_s^2 = 1/3$ [75]. The two solar mass requirements, according to several studies [75, 76, 77], necessitates a speed of sound squared that exceeds the conformal limit ($c_s^2 = 1/3$), revealing that the matter inside of NS is a highly interacting system. In Figure 2, the c_s^2 for pure nucleonic matter is significantly high, around 0.75, for the maximum mass configuration. In the appearance of different particles, such as hyperons, we can see the kinks corresponding to the onset of a new particle species, resulting in noticeable changes in the speed of sound squared. The value decreases to 0.54 for nucleonic EoS with hyperons.

With the phase transition to the quark matter, c_s^2 drops to zero in the mixed-phase region because the pressure remains constant and then increases again in the pure quark phase. For hybrid EoS with nucleons only, we see that the speed of sound squared increases to higher values when it is still in the pure hadronic phase. Within the mixed-phase region, which extends from number density $n_b = 0.56$ fm⁻³ to $n_b = 0.74$ fm⁻³, the speed of sound squared remains zero. After the phase transition, it drops to a value of 0.27 at the maximum mass configuration, which lies in the pure quark phase. For the hybrid EoS with nucleons and hyperons, the mixed-phase region is very small, $n_b = 0.57$ - 0.59 fm⁻³, and the maximum speed of sound squared is 0.25. At high energy densities, all speed of sound value stays well below the conformal limit, unlike previous observations, due to the expected approach of a deconfined EoS towards the conformal limit from below.

Figure 3 illustrates the mass-radius relationship based on so-

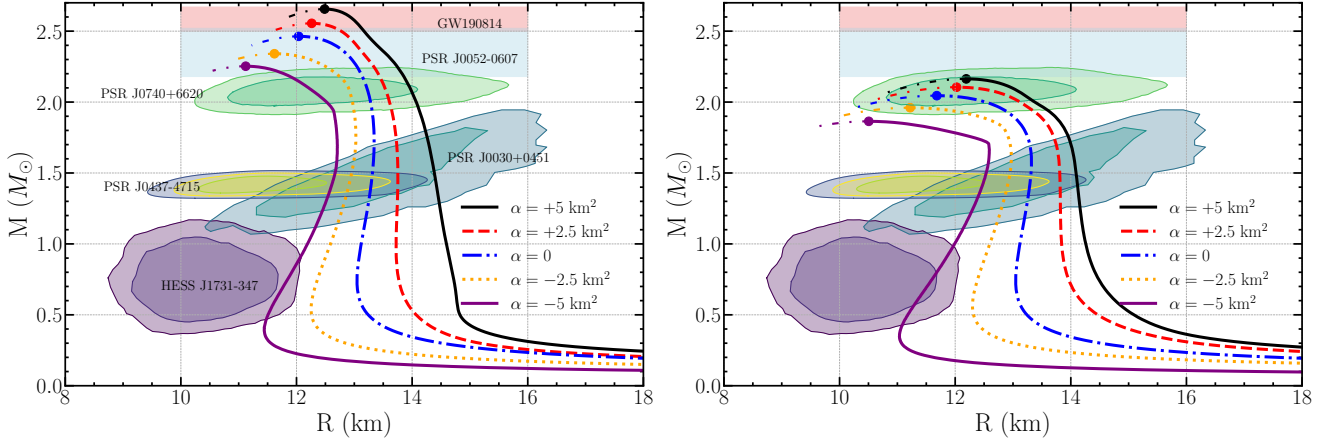


Figure 3: Left: Mass-Radius relation for the nucleonic matter (left) and nucleons with hyperons (right) at different values of α . The various shaded areas are credibility regions from the mass and radius inferred from the analysis of GW190814, PSR J0952-0607, PSR J0740+6620, PSR J0030+0451, PSR J0437-4715, and HESS J1731-347 [78, 79, 80, 48, 49, 51, 52].

lutions of the modified TOV equations for N (left) and N + H (right) EoSs at different values of the GB constant α . The solid dot represents the last stable point reached in the center of the maximum-mass solution of the TOV equation. The dash-dotted line after the solid dot corresponds to the unstable part. In the left plot, for pure nucleonic matter, the maximum mass reaches $2.46 M_{\odot}$ with a radius of 12.04 km for $\alpha = 0$, which resembles the MR relation obtained by solving the TOV equations for the equilibrium structure of an NS [81]. With the negative values of α (km^2), the MR relation shifts to a low radius and hence low maximum mass. For $\alpha = -2.5$ and -5.0 km^2 , the maximum mass decreases to 2.34 and $2.25 M_{\odot}$, respectively. The radius at $1.4 M_{\odot}$ decreases to 12.90 and 12.60 km, respectively, for $\alpha = -2.5$ and 5.0 km^2 . While the standard $\alpha = 0$ satisfies the astrophysical constraints from several measurements, the MR relation for $\alpha = -5.0 \text{ km}^2$ satisfies the low mass HESS J1731-347 constraint, thereby explaining its nature to be a hadronic star. For positive values of GB constant, the maximum mass increases to a value of 2.55 and $2.65 M_{\odot}$ for $\alpha = +2.5$ and $+5.0 \text{ km}^2$, respectively. These values of the maximum mass satisfies the GW190814 constraint [79] which lies in the so-called mass gap region. This suggests that the nature of the secondary component of GW190814 could be a supermassive NS.

For the EoS with nucleons and hyperons, the maximum mass for $\alpha = 0$ is $2.04 M_{\odot}$ with a radius of 13.28 km at $1.4 M_{\odot}$. For $\alpha = -2.5$ and -5.0 km^2 , the maximum mass decreases to 1.96 and $1.86 M_{\odot}$, respectively. These values lie well below the $2.0 M_{\odot}$ limit which is a requirement to describe the NSs. So in the case of N + H EoS, the negative values can be ignored in terms of satisfying the astrophysical constraints. For positive values, the maximum mass increases to a value of 2.10 and $2.16 M_{\odot}$ for $\alpha = +2.5$ and $+5.0 \text{ km}^2$, respectively.

Figure 4 shows the mass-radius relation at different GB constant α for nucleonic (left) and hyperonic (right) EoS with a phase transition to the quark matter at different quark model parameters (C , $D^{1/2}$). For the hybrid EoS with nucleons only at $\alpha = 0$, the maximum mass is $2.29 M_{\odot}$ with a radius of 13 km resembling the MR relation obtained by solving the TOV equa-

tions for the equilibrium structure of an NS [70]. With negative values of α , the maximum mass decreases to around $1.93 M_{\odot}$, lying below the $2.0 M_{\odot}$ limit. The radius at $1.4 M_{\odot}$ decreases to a value of 12.66 km for $\alpha = -5.0 \text{ km}^2$. With positive values, a maximum mass of $2.50 M_{\odot}$ and a radius of 14.13 km is obtained at $1.4 M_{\odot}$, satisfying all the necessary astrophysical constraints.

For the hybrid EoS with nucleons and hyperons, the maximum mass is $1.95 M_{\odot}$ with a radius of 12.54 km. Despite selecting quark parameters for a stiff EoS, including hyperons and a phase transition to quark matter leads to an EoS that softens enough to limit the star's maximum mass to slightly under $2 M_{\odot}$. This is because of the initial low value of the maximum mass for the EoS without a phase transition. The maximum mass value decreases to $1.71 M_{\odot}$ for $\alpha = -5.0 \text{ km}^2$, satisfying the HESS J1731-347 constraint, and $2.20 M_{\odot}$ for $\alpha = +5.0 \text{ km}^2$, satisfying the necessary $2 M_{\odot}$ and other NICER measurements. In both the hybrid EoSs, the phase transition occurs at a very high density, allowing for a very small amount of quark matter in the core.

The above plots showed how the GB constant α affects the overall MR relation at certain values. In order to see a more general behavior, we calculated the MR relation for several values of $\alpha = 0, -1.0, -2.0, -2.5, -3.0, -4.0, -5.0 \text{ km}^2$, and the corresponding positive values. We calculated the maximum mass and the corresponding radius for all the values, and plotted them with some fit functions, to see a general behavior.

Figure 5 displays the variation of the maximum mass for different compositions of the EoS without and with phase transition, at different values of the GB constant α . We see that the maximum mass increases for positive values of α and vice-versa for negative values. The change in the maximum mass for nucleonic EoS without and with phase transition keeps increasing with the increase in the value of α . For the hyperonic EoS at higher values, with and without a phase transition, the maximum mass changes slightly. At $\alpha = +4.0$ and $+5.0 \text{ km}^2$, the hybrid EoS results in more massive stars than those without a phase transition.

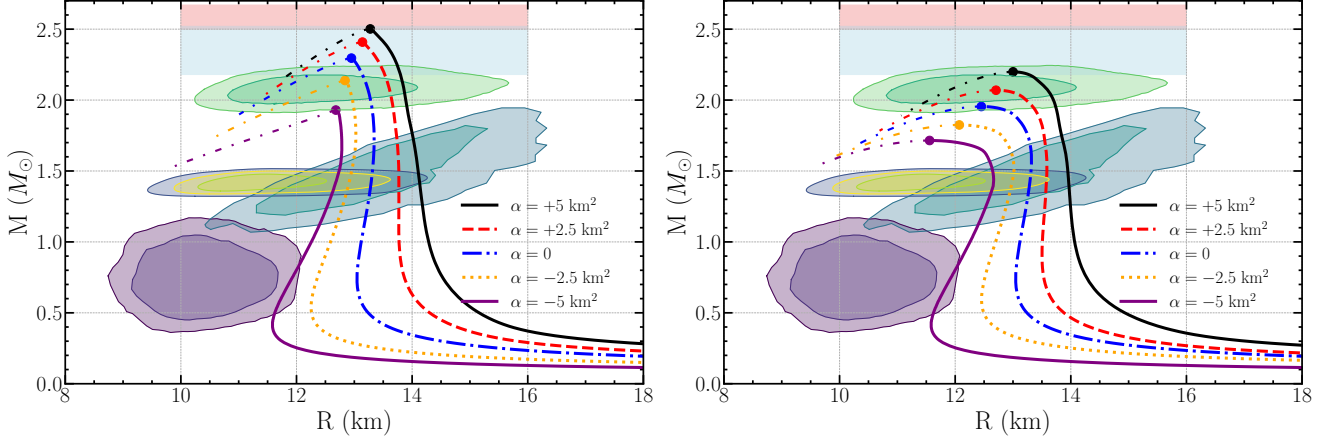


Figure 4: Same as Figure 3, but with a phase transition to the quark matter at different quark model parameters ($C, D^{1/2}$).

To fit the function between maximum mass and the constant α , we use the following form

$$M = a.(k.x)^2 + b.(k.x) + c \quad (39)$$

Here k is the scaling factor. As we can see from the plot, all the EoS satisfy the fit functions pretty accurately. The values of the constants and scaling factors for different EoSs are shown in Table 3.

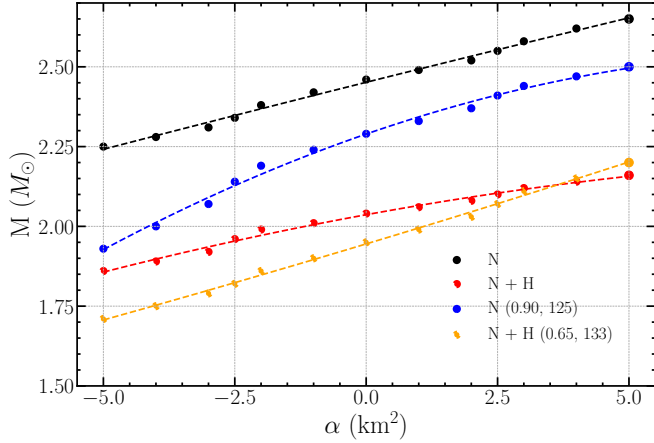


Figure 5: Variation of the maximum mass for different compositions of the EoS without and with phase transition, at different values of the GB constant α .

Table 3: Values of fitting coefficients for Eq. 39.

EoS	$a (M_\odot)$	$b (M_\odot)$	$c (M_\odot)$	$k (km^{-2})$
N	1.08×10^2	33.74	2.45	1.22×10^{-3}
N + H	3.69×10^3	53.08	2.04	5.66×10^{-4}
N (0.90, 125)	2.67×10^2	16.67	2.29	3.4×10^{-3}
N + H (0.65, 133)	5.59×10^1	19.26	1.94	2.57×10^{-3}

The same analysis is performed for the maximum radius at different values of α . For the radius, we fit the following function:

$$R = a.(k.x)^2 + b.(k.x) + c \quad (40)$$

Figure 6 shows the change in the maximum radius for different compositions of the EoS without and with phase transition, at different values of the GB constant α . From the plot, we see that the initial radius for hybrid EoSs at $\alpha = 0$ is higher than the EoS without a phase transition. For pure nucleonic EoS without a phase transition, the radius varies from 11.12 to 12.49 km for $\alpha = -5.0$ and $+5.0$ km², respectively. For the hybrid nucleonic EoS, this changes from 12.68 km to 13.27 km, respectively. So while the maximum radius for hybrid nucleonic EoSs is higher than the normal nucleonic EoS, the change in the radius is large for EoSs without a phase transition. Similar behavior is seen for the EoS with hyperons. The values of different constants and the scaling factor for different EoSs are shown in Table 4.

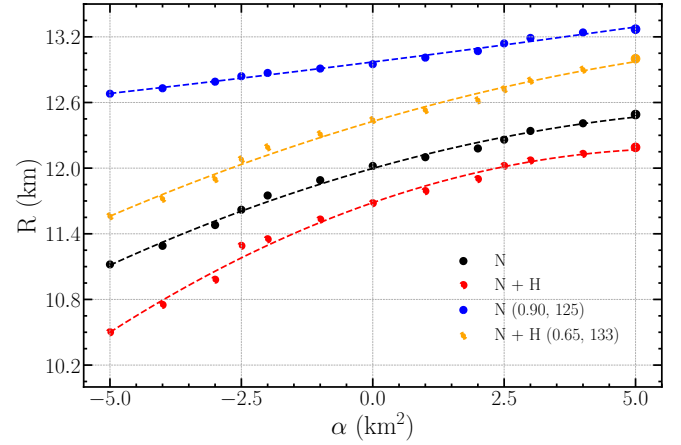


Figure 6: Same as Figure 5, but for the maximum radius).

Table 4: Same as Table 3, but for Eq. 40.

EoS	$a (km^{-1})$	b	$c (km)$	$k (km^{-1})$
N	3.39×10^2	2.74×10^1	12.0	4.94×10^{-3}
N + H	5.58×10^2	3.33×10^1	11.68	5.01×10^{-3}
N (0.90, 125)	1.73×10^4	3.15×10^2	12.97	1.92×10^{-4}
N + H (0.65, 133)	1.49×10^4	2.15×10^2	12.43	6.56×10^{-4}

5. Summary and Conclusion

To summarize our work, in the present study, we have investigated in detail the impact of hyperons on the structural properties of hadronic and hybrid stars within the framework of the Einstein-Gauss-Bonnet theory of gravity in four-dimensional space-time. We briefly presented the action of the modified theory of gravity, the corresponding field equations, as well as the modified TOV equations for static, spherically symmetric stars. We discussed and described the formalism to obtain a realistic hadronic EoS compatible with astrophysical constraints, including hyperons within the relativistic mean field theory, which guarantees that causality is never violated. Deconfined quark matter and phase transition were discussed as well. We have integrated the equations numerically, assuming both negative and positive values of the Gauss-Bonnet coupling constant within its allowed range, and we have displayed our main numerical results in several tables and figures.

Our results show that the inclusion of hyperons softens the EoS, while the phase transition softens it even further. The speed of sound squared throughout the density range remains always positive and lower than unity, avoiding causality. As far as the mass-radius relationships are concerned, we observed that i) For a given stellar mass, a positive Gauss-Bonnet coupling constant α implies massive stars satisfying several astrophysical constraints that cannot be fulfilled with a standard EoS. The negative coupling implies smaller stars. Even though they satisfy and explain the low-mass measurements, such as HESS J1731-347, the maximum mass is smaller than the $2 M_{\odot}$ limit and hence can be ruled out. ii) The inclusion of hyperons, since the EoS becomes softer, implies a lower highest stellar mass, as was expected. A few concrete examples of M, R pairs (highest stellar mass and corresponding radius) have been given in the text. iii) Fitting to the maximum mass and corresponding radius for several values of constant α provides a general behavior of change in these properties.

Regarding future work, a natural extension of this study would be to add other Δ baryons, compute the M-R relationships, as well as the tidal Love numbers and dimensionless tidal deformability.

Acknowledgement

I.A.R. acknowledges support from the Alexander von Humboldt Foundation.

References

- [1] T. Kaluza, Sitzungsber. Preuss. Akad. Wiss. Berlin (Math. Phys.) **1921**, 966-972 (1921) [arXiv:1803.08616 [physics.hist-ph]].
- [2] O. Klein, Z. Phys. **37**, 895-906 (1926).
- [3] H. P. Nilles, Phys. Rept. **110**, 1-162 (1984).
- [4] M. B. Green, J. H. Schwarz and E. Witten, *Superstring Theory, Vol. 1 & 2*, Cambridge Monographs on Mathematical Physics (Cambridge University Press, Cambridge, England, 2012).
- [5] J. Polchinski, *String Theory, Vol. 1 & 2*, Cambridge Monographs on Mathematical Physics (Cambridge University Press, Cambridge, England, 2005).
- [6] D. Lovelock, J. Math. Phys. **12**, 498-501 (1971).
- [7] S. Corley, D. A. Lowe and S. Ramgoolam, JHEP **07**, 030 (2001) [arXiv:hep-th/0106067 [hep-th]].
- [8] D. Glavan and C. Lin, Phys. Rev. Lett. **124**, 081301 (2020).
- [9] R. P. Woodard, Scholarpedia **10**, 32243 (2015). [arXiv:1506.02210 [hep-th]].
- [10] S. G. Ghosh and R. Kumar, Class. Quant. Grav. **37**, 245008 (2020). [arXiv:2003.12291 [gr-qc]].
- [11] R. A. Konoplya and A. Zhidenko, Phys. Dark Univ. **30**, 100697 (2020). [arXiv:2003.12492 [gr-qc]].
- [12] D. V. Singh and S. Siwach, Phys. Lett. B **808**, 135658 (2020). [arXiv:2003.11754 [gr-qc]].
- [13] S. A. Hosseini Mansoori, Phys. Dark Univ. **31**, 100776 (2021). [arXiv:2003.13382 [gr-qc]].
- [14] D. V. Singh, S. G. Ghosh and S. D. Maharaj, Phys. Dark Univ. **30**, 100730 (2020).
- [15] S. W. Wei and Y. X. Liu, Phys. Rev. D **101**, 104018 (2020).
- [16] K. Yang, B. M. Gu, S. W. Wei and Y. X. Liu, Eur. Phys. J. C **80**, 662 (2020).
- [17] P. G. S. Fernandes, Phys. Lett. B **805**, 135468 (2020).
- [18] C. Y. Zhang, S. J. Zhang, P. C. Li and M. Guo, JHEP **2008**, 105 (2020).
- [19] K. Jusufi, Annals Phys. **421**, 168285 (2020).
- [20] A. Abdujabbarov, J. Rayimbaev, B. Turimov and F. Atamurotov, Phys. Dark Univ. **30**, 100715 (2020).
- [21] K. Jafarzade, M. Kord Zangeneh and F. S. N. Lobo, arXiv:2009.12988 [gr-qc].
- [22] S. U. Islam, R. Kumar and S. G. Ghosh, JCAP **2009**, 030 (2020).
- [23] X. H. Jin, Y. X. Gao and D. J. Liu, Int. J. Mod. Phys. D **29**, 2050065 (2020).
- [24] R. Kumar, S. U. Islam and S. G. Ghosh, Eur. Phys. J. C **80**, 1128 (2020).
- [25] M. S. Churilova, Phys. Dark Univ. **31**, 100748 (2021).
- [26] A. K. Mishra, Gen. Rel. Grav. **52**, 106 (2020).
- [27] A. Aragon, R. Becar, P. A. Gonzalez and Y. Vasquez, Eur. Phys. J. C **80**, 773 (2020).
- [28] R. A. Konoplya and A. F. Zinhailo, Eur. Phys. J. C **80**, 1049 (2020).
- [29] M. Guo and P. C. Li, Eur. Phys. J. C **80**, 588 (2020).
- [30] X. X. Zeng, H. Q. Zhang and H. Zhang, Eur. Phys. J. C **80**, 872 (2020).
- [31] K. Jusufi, A. Banerjee and S. G. Ghosh, Eur. Phys. J. C **80**, 698 (2020).
- [32] P. Liu, C. Niu, X. Wang and C. Y. Zhang, arXiv:2004.14267 [gr-qc].
- [33] L. M. Cao and L. B. Wu, [arXiv:2103.09612 [gr-qc]].
- [34] D. Wang and D. Mota, Phys. Dark Univ. **32**, 100813 (2021). [arXiv:2103.12358 [astro-ph.CO]].
- [35] J. X. Feng, B. M. Gu and F. W. Shu, Phys. Rev. D **103**, 064002 (2021). [arXiv:2006.16751 [gr-qc]].
- [36] T. Clifton, P. Carrilho, P. G. S. Fernandes and D. J. Mulryne, Phys. Rev. D **102**, 084005 (2020). [arXiv:2006.15017 [gr-qc]].
- [37] N. K. Glendenning, Compact stars: Nuclear physics, particle physics, and general relativity, 1997.
- [38] I. Bombaci, in: Proceedings of the 12th International Conference on Hypernuclear and Strange Particle Physics (HYP2015, 2017, p. 101002. doi:10.7566/JPSCP.17.101002.
- [39] B. P. Abbott, R. Abbott *et al.*, Phys. Rev. Lett. **119** (2017) 161101. URL: <https://link.aps.org/doi/10.1103/PhysRevLett.119.161101>. doi:10.1103/PhysRevLett.119.161101.
- [40] C. D. Capano, I. Tews, S. M. Brown, B. Margalit, S. De, S. Kumar, D. A. Brown, B. Krishnan, S. Reddy, Nature Astronomy **4** (2020) 625-632. URL: <https://doi.org/10.1038/s41550-020-1014-6>. doi:10.1038/s41550-020-1014-6.
- [41] P. Demorest, T. Pennucci, S. Ransom, M. Roberts, J. Hessels, Nature **467** (2010) 1081-1083. doi:10.1038/nature09466. arXiv:1010.5788.
- [42] J. Antoniadis, *et al.*, Science **340** (2013) 6131. doi:10.1126/science.1233232. arXiv:1304.6875.
- [43] E. Fonseca, *et al.*, Astrophys. J. Lett. **915** (2021) L12. doi:10.3847/2041-8213/ac03b8. arXiv:2104.00880.
- [44] T. E. Riley, *et al.*, Astrophys. J. Lett. **918** (2021) L27. doi:10.3847/2041-8213/ac0a81. arXiv:2105.06980.
- [45] M. C. Miller, *et al.*, The Astrophysical Journal Letters **918** (2021) L28. URL: <https://dx.doi.org/10.3847/2041-8213/ac089b>. doi:10.3847/2041-8213/ac089b.
- [46] T. Salmi, *et al.*, Astrophys. J. **974** (2024) 294. doi:10.3847/1538-4357/ad5f1f. arXiv:2406.14466.

- [47] A. J. Dittmann, et al. (2024). URL: <https://arxiv.org/abs/2406.14467>. arXiv:2406.14467.
- [48] M. C. Miller *et al.*, *Astrophys. J.* 887 (2019) L24. URL: <https://doi.org/10.3847/2041-8213/ab50c5>. doi:10.3847/2041-8213/ab50c5.
- [49] T. E. Riley *et al.*, *Astrophys. J.* 887 (2019) L21. URL: <https://doi.org/10.3847/2041-8213/ab481c>. doi:10.3847/2041-8213/ab481c.
- [50] S. Vinciguerra, et al., *Astrophys. J.* 961 (2024) 62. doi:10.3847/1538-4357/acfb83. arXiv:2308.09469.
- [51] D. Choudhury, et al. (2024). arXiv:2407.06789.
- [52] V. Doroshenko, V. Suleimanov, G. Pühlhofer, A. Santangelo, *Nature Astronomy* 6 (2022) 1444–1451. URL: <https://doi.org/10.1038/s41550-022-01800-1>. doi:10.1038/s41550-022-01800-1.
- [53] Y. Kini, et al. (2024). arXiv:2405.10717.
- [54] T. Tangphati, A. Pradhan, A. Banerjee and G. Panotopoulos, *Phys. Dark Univ.* 33, 100877 (2021) [arXiv:2109.00195 [gr-qc]].
- [55] A. Banerjee, T. Tangphati, D. Samart and P. Channuie, *Astrophys. J.* **906**, no.2, 114 (2021) [arXiv:2007.04121 [gr-qc]].
- [56] G. Panotopoulos, A. Pradhan, T. Tangphati and A. Banerjee, *Chin. J. Phys.* **77**, 2106-2114 (2022).
- [57] R. Brockmann, H. Toki, *Phys. Rev. Lett.* 68 (1992) 3408–3411. URL: <https://link.aps.org/doi/10.1103/PhysRevLett.68.3408>. doi:10.1103/PhysRevLett.68.3408.
- [58] M. Dutra, O. Lourenço, S. Avancini, B. Carlson, A. Delfino, D. Menezes, C. Providência, S. Typel, J. Stone, *Physical Review C* 90 (2014) 055203. URL: <https://link.aps.org/doi/10.1103/PhysRevC.90.055203>. doi:10.1103/PhysRevC.90.055203.
- [59] M. Oertel, M. Hempel, T. Klähn, S. Typel, *Rev. Mod. Phys.* 89 (2017) 015007. doi:10.1103/RevModPhys.89.015007.
- [60] L. L. Lopes, K. D. Marquez, D. P. Menezes, *Physical Review D* 107 (2023) 036011. URL: <https://link.aps.org/doi/10.1103/PhysRevD.107.036011>. doi:10.1103/PhysRevD.107.036011.
- [61] A. Issifu, K. D. Marquez, M. R. Pelicer, D. P. Menezes (2023). arXiv:2302.04364.
- [62] S. Typel, H. H. Wolter, *Nucl. Phys. A* 656 (1999) 331–364. doi:10.1016/S0375-9474(99)00310-3.
- [63] C. Fuchs, H. Lenske, H. H. Wolter, *Phys. Rev. C* 52 (1995) 3043–3060. URL: <https://link.aps.org/doi/10.1103/PhysRevC.52.3043>. doi:10.1103/PhysRevC.52.3043.
- [64] B. C. Backes, K. D. Marquez, D. P. Menezes, *The European Physical Journal A* 57 (2021) 1–9.
- [65] C. J. Xia, G. X. Peng, S. W. Chen, Z. Y. Lu, J. F. Xu, *Phys. Rev. D* 89 (2014) 105027. URL: <https://link.aps.org/doi/10.1103/PhysRevD.89.105027>. doi:10.1103/PhysRevD.89.105027.
- [66] D. Logoteta, I. Bombaci, *Phys. Rev. D* **88** (2013) 063001. URL: <https://link.aps.org/doi/10.1103/PhysRevD.88.063001>. doi:10.1103/PhysRevD.88.063001.
- [67] N. K. Glendenning, *Phys. Rev. D* 46 (1992) 1274–1287. doi:10.1103/PhysRevD.46.1274.
- [68] I. A. Rather, A. A. Usmani, S. K. Patra, *J. Phys. G* 48 (2021) 085201. doi:10.1088/1361-6471/ac0129. arXiv:2011.14077.
- [69] I. A. Rather, U. Rahaman, M. Imran, H. C. Das, A. A. Usmani, S. K. Patra, *Phys. Rev. C* 103 (2021) 055814. doi:10.1103/PhysRevC.103.055814. arXiv:2102.04067.
- [70] I. A. Rather, K. D. Marquez, B. C. Backes, G. Panotopoulos, I. Lopes, *JCAP* 05 (2024) 130. doi:10.1088/1475-7516/2024/05/130. arXiv:2401.07789.
- [71] G. Baym, C. Pethick, P. Sutherland, *Astrophys. J.* 170 (1971) 299–317. doi:10.1086/151216.
- [72] S. S. Avancini, L. Brito, J. R. Marinelli, D. P. Menezes, M. M. W. de Moraes, C. Providência, A. M. Santos, *Phys. Rev. C* 79 (2009) 035804. URL: <https://link.aps.org/doi/10.1103/PhysRevC.79.035804>. doi:10.1103/PhysRevC.79.035804.
- [73] H. Pais, C. m. c. Providência, *Phys. Rev. C* 94 (2016) 015808. URL: <https://link.aps.org/doi/10.1103/PhysRevC.94.015808>. doi:10.1103/PhysRevC.94.015808.
- [74] I. A. Rather, A. Usmani, S. Patra, *Nuclear Physics A* 1010 (2021) 122189. URL: <https://www.sciencedirect.com/science/article/pii/S0375947421000543>. doi:https://doi.org/10.1016/j.nuclphysa.2021.122189.
- [75] P. Bedaque, A. W. Steiner, *Phys. Rev. Lett.* 114 (2015) 031103. URL: <https://link.aps.org/doi/10.1103/PhysRevLett.114.031103>. doi:10.1103/PhysRevLett.114.031103.
- [76] C. C. Moustakidis, T. Gaitanos, C. Margaritis, G. A. Lalazissis, *Phys. Rev. C* 95 (2017) 045801. URL: <https://link.aps.org/doi/10.1103/PhysRevC.95.045801>. doi:10.1103/PhysRevC.95.045801.
- [77] I. Tews, J. Carlson, S. Gandolfi, S. Reddy, *The Astrophys. J.* 860 (2018) 149. URL: <https://dx.doi.org/10.3847/1538-4357/aac267>. doi:10.3847/1538-4357/aac267.
- [78] R. W. Romani, D. Kandel, A. V. Filippenko, T. G. Brink, W. Zheng, *Astrophys. J. Lett.* 934 (2022) L17. doi:10.3847/2041-8213/ac8007. arXiv:2207.05124.
- [79] R. Abbott, et al. (LIGO Scientific, Virgo), *Astrophys. J. Lett.* 896 (2020) L44. doi:10.3847/2041-8213/ab960f.
- [80] T. E. Riley, et al., *The Astrophysical Journal Letters* 918 (2021) L27. URL: <https://dx.doi.org/10.3847/2041-8213/ac0a81>. doi:10.3847/2041-8213/ac0a81.
- [81] I. A. Rather, K. D. Marquez, G. Panotopoulos, I. Lopes, *Phys. Rev. D* 107 (2023) 123022. doi:10.1103/PhysRevD.107.123022. arXiv:2303.11006.